Biogeosciences Discuss., 9, 2233–2276, 2012
www.biogeosciences-discuss.net/9/2233/2012/
doi:10.5194/bgd-9-2233-2012

Biogeosciences Discussions

Biogeochemistry of an amazonian podzol-ferralsol soil system with white kaolin

Y. Lucas[1], C. R. Montes[2], S. Mounier[1], M. Loustau-Cazalet[1,*], D. Ishida[3,], R. Achard[1,***], C. Garnier[1], and A. J. Melfi[4]**

[1]PROTEE, Université du Sud Toulon-Var, La Garde, Toulon, France
[2]NUPEGEL, CENA, Universidade de São Paulo, Piracicaba, Brazil
[3]NUPEGEL, IG, Universidade de São Paulo, São Paulo, Brazil
[4]NUPEGEL, ESALQ, Universidade de São Paulo, Piracicaba, Brazil
[*]now at: LGCIE, INSA, Université de Lyon, Villeurbanne, France
[**]now at: NUPEGEL, CENA, Universidade de São Paulo, Piracicaba, Brazil
[***]now at: INERIS, Aix-en-Provence, France

Received: 23 December 2011 – Accepted: 2 February 2012 – Published: 28 February 2012

Correspondence to: Y. Lucas (lucas@univ-tln.fr)

Published by Copernicus Publications on behalf of the European Geosciences Union.

Abstract

Podzol-ferralsol soil systems cover great areas in Amazonia and in other equatorial regions, they are an end-member of old equatorial landscape evolution, are frequently associated with kaolin deposits and store and export large amounts of carbon. Their biogeochemistry was usually inferred from soil mineralogy and from spring or river water properties. This paper presents a database for groundwaters sampled in situ in a typical podzol-ferralsol soil catena from the Alto Rio Negro region, Brazil; the sampling periods allowed to sample under high- and low-level water-table conditions. The compositions of the groundwaters percolating the soil system are consistent with the currently observed mineral and organic paragenesis.

The acidity and the site density of the dissolved organic matter (DOM) produced and circulating in the podzol white sand horizons are similar to what was observed in acid podzolic temperate zone. The aggressiveness of the white sand groundwater with regard to secondary minerals favours the podzol development at the expense of the ferralsolic or kaolin material.

Some DOM is able to percolate in depth through clayey material with concentrations up to 9.7 $mgC\,l^{-1}$ (4.0 on average). This DOM is characterized by high site densities indicating a large proportion of small carboxylic acids.

In the deep kaolin and in the ferralsolic horizons, the Si and Al content of the groundwater is controlled by gibbsite and kaolinite precipitation/dissolution and by quartz dissolution. The mobility of Fe, mainly transported as Fe^{2+}, is sensitive to small variations in E_H. The bleaching of the deep kaolin at the upper part of the slopes is favoured by the high content of small carboxylic compounds and by the redox conditions of the solutions issuing from the podzolic horizons. The transfer of Al and Fe result in the precipitation of Al-nodules in slope horizons and of Fe-oxides in the upper downslope horizon.

It can be inferred that thick bleached kaolin are likely everywhere presently active giant podzols are close to a slope gradient sufficient to allow deep percolation of groundwater.

BGD

9, 2233–2276, 2012

1 Introduction

More than 18 % of the Amazonian area is covered by podzol-ferralsol systems (RadamBrasil, 1978), which are characterized by the juxtaposition of podzols and ferralsols on the same landscape units (Lucas et al., 1984; Chauvel et al., 1987). Ferralsols are usual, climacic soils of equatorial areas where high weathering rates and long time of evolution allowed the leaching of all major elements but Al, Fe and Ti, the persistence of Si as kaolinite in the upper horizons being allowed by plant cycling (Lucas et al., 1993). The podzols appear and develop where dissolved organic matter (DOM) is able to percolate through soil horizons down to the rivers, allowing Al and Fe leaching and thus favouring the dissolution of clay and iron oxides (Lucas et al., 1996; Lundström et al., 2000; Nascimento et al., 2004). Once initiated, this process induces a positive feed-back and the progressive replacement of the ferralsols by podzols, even where ferralsols are clayey; large podzol areas constitute thus one end-member of equatorial soils and landscape evolution (Dubroeucq and Volkoff, 1998) (Fig. 1).

The podzolic areas of such systems have the ability to release great amounts of dissolved organic carbon (DOC) (Leenheer, 1980; Chauvel et al., 1996; Benedetti et al., 2003; Patel-Sorrentino et al., 2007) in the draining waters, allowing its transfer to the sea by rivers. Considering the Amazon basin, they provide a tenth of the 0.13 PgC annually exported to the sea (Tardy et al., 2009). They also can store large amounts of carbon in the upper and the deep Bh and Bhs horizons (Batjes et Dijkshoorn, 1999; Bernoux et al., 2002; Veillon and Soria-Solano, 1988; Nascimento et al., 2004; Montes et al., 2011). According to these last authors, hydromorphic podzols can store 86.8 ± 7.1 kgC m^{-2} and at least 13.6 ± 1.1 PgC is stored in Amazonian podzols and could return the atmosphere if the climate changes with the onset of a dry season. These soil systems thus take a significant part to the CO_2 cycle at the global scale, but the dynamics of DOM transfer and accumulation is still poorly known.

Podzol-ferralsol systems are also frequently associated with kaolin deposits (Montes et al., 2007). Thick kaolin horizons (up to 10 m thick) were found below the Bh-Bs

BGD
9, 2233–2276, 2012

horizons situated at the bottom of the thick, eluviated white sand horizons of the podzols. The genetic relationships between podzols and kaolin and the specific role of the DOM in the system dynamics was recently considered by Montes et al. (2007), who hypothesized that the mineralization of the Bh-Bhs organic matter at depth turns the acidic percolating water more reductive, favouring the leaching of the iron and allowing the bleaching of the kaolin horizons. Their hypothesis, however, needs to be assessed by more detailed geochemical characterizations. Several detailed studies of the solid mineral and organic phases have already been conducted on Amazonian podzols (Bravard and Righi, 1991; Nascimento et al., 2004; Bardy et al., 2008; Fritsch et al., 2009), but the properties or composition of the circulating solutions were only inferred from the properties of solid phases. Few works (Cornu et al., 1997, 1998; Nascimento et al., 2008) have focused on sampling and studying the percolating solutions, mainly because of difficulties of sampling groundwater in these regions. More generally, except for the surface horizons little is directly known about percolating soil solution in humid tropic soils.

In this context, the aim of the paper is to understand (1) the relationships between soil water and soil mineralogy in such systems, especially with regard to kaolin genesis, (2) the specific role of DOM and (3) the processes which define the spring water characteristics, on the base of a detailed study of a podzol-ferralsols catena. Such knowledge is necessary to evaluate the possible changes in the natural organic matter (NOM) dynamics through global change, as well as to understand the relationships between soil, kaolin and landscape features, in order to preview the soil characteristics and the possibility of kaolin ore from remote sensing.

BGD
9, 2233–2276, 2012

2 Material and methods

2.1 Description of the studied area

The studied soil catena is situated near the São Gabriel da Cachoeira city, Amazonas state, Brazil, at 0°6′21″ S and 66°54′22″ W (Fig. 1), and was described in previous publications (Montes et al., 2007; Ishida, 2010). It cuts the edge of a plateau where giant podzols developed from the plateau centre at the expense of reddish yellow, low activity clay ferralsols, as described elsewhere (Lucas et al., 1988; Dubroeucq and Volkoff, 1998). It is related to a river network which enters the plateau by regressive erosion.

The climate is typically equatorial, with an annual rainfall around 3000 mm and without a marked dry season. Daily rainfall data were obtained from the airport station situated 6 km from the studied area. The geological substratum is composed of crystalline rocks having composition varying between monzogranitic, sienogranitic and quartzomonzonitic (Dall'Agnol and Macambira, 1992). The vegetation over the ferralsols and over well-drained podzols is a typical lowland tropical evergreen forest and over the hydromorphic podzols a specific forest called *campinarana* and characterized by a high density of smaller trees (20–30 m).

The soils were studied using a structural analysis approach (Boulet et al., 1982; Fritsch and Fitzpatrick, 1994; Delarue et al., 2009). Macromorphological features were observed through boreholes and pit descriptions. Mineralogy was determined by X-ray diffraction on powder samples, diffuse reflectance spectroscopy and thermogravimetric analysis. Only the data necessary to understand the water geochemistry are given here; detailed mineralogy and geochemistry are given in Ishida (2010).

The soil catena (length 200 m, difference in altitude 15 m) is sketched on Fig. 2. Two main sets of horizons can be distinguished: (1) the horizons of the well-expressed podzols, at the upper part of the catena, and (2) the oxic horizons coloured by Fe-oxides on the slopes. Thick kaolin horizons were observed below both podzolic and oxic horizons. The main minerals found in each horizon were identified and quantified

BGD
9, 2233–2276, 2012

by X-ray diffraction, differential gravimetric and thermic analysis, diffuse reflectance spectroscopy and chemical analysis (Ishida, 2010). Results are summarized in Table 1.

The podzols have a typical vertical succession of horizons: O, A1, E, Bh, Bhs. The organic O horizons are peat-like, with a thickness varying from a few centimetres to more than 50. The more water-logged the topsoil throughout the year, i.e. far from the plateau slopes, the thicker the O horizons. The humic A1 horizons are well-developed; they consist of clean white quartz sand and organic matter particles. The eluviated sandy Es horizons have thin (1–2 mm), dark-grey micro-horizons coloured by organic matter particles; they have traces of kaolinite and gibbsite and high porosity and hydraulic conductivity. The transition between Es horizons and the underlying kaolin shows the vertical following sequence: (1) Bh – the sandy Es horizon turns progressively darker, due to an increase of organic matter content; (2) Bhs – there is an irregular, finger-like transition towards a hardened, sandy-clay horizon, brown coloured (10YR 5/2) (colors are given according to Munsell, 1990) with dark brown (7.5YR 5/6) features formed by organic matter and Fe-oxides accumulation in cracks and tubular pores, the gibbsite content is higher, the quartz sand content diminishes quickly in depth, together with the increase of kaolinite and the hydraulic conductivity turns lower. The kaolin K1 and K2 horizons consist mainly of kaolinite, with gibbsite content around 8 % at the upper part of K1 and decreasing in depth to be lower than 2 % at the lower part of K2 (Fig. 3). The upper part of the kaolin is a clayey, whitish material with some orange-coloured coatings in tubular pores (K1 horizon). These coatings progressively diminish in depth, giving place to a homogeneous, white, clayey, butter-like material (K2 horizon). In depth, the C1 horizon is a silt-clay saprolite having muscovite and weathered feldspar.

Going downslope, podzolic horizons give place to oxic horizons coloured by Fe-oxides: A horizons, on the upper part of the profiles; B1 horizons, which progressively changes from sandy to sandy-clay in the downslope direction; B2 sandy-clay horizons; B3 horizons in the downslope position having water-logging features. Below the B1 horizon were observed a silty clay loam, pale yellow horizon with coarse quartz grains

BGD
9, 2233–2276, 2012

(Ef). It indicates a perched water-table and is associated with small micro-valleys (2 to 4 m wide and 1 to 2 m depth) whose the flat bottom is at the same altitude than the Ef horizon, the micro-valleys forming a hydrographical network on the slopes. In depth the thick kaolin horizons, the clayey K1 and K2 horizons extend downslope. The colours are yellow (10YR 8/6) and white (5Y 8/1 to 5Y 8/2), for K1 and K2 horizons, respectively. A K3 horizon having some remaining quartz grains and some red and yellow nodules appears at the mid-slope at the upper part of the kaolin corp. Downslope, the K1 and K2 horizons give place to the K4 horizon characterized by more abundant unweathered muscovites and Fe red spots at its upper part. Gibbsitic nodules are located at the downslope half of the catena as indicated on the figure. In depth, C1 and C2 horizons are saprolitic horizons having many muscovite and weathered feldspar. At the lower part of the catena, the water table had the typical odour of sulphurs.

2.2 Water sampling and analysis

2.2.1 Lysimeters and sampling points

It appeared unnecessary for the purpose of the present work to collect and analyze rain openfall, troughfall and stemflow. Such a study is difficult because of highly spatial variability under forest cover and had already been conducted in a similar podzol-ferralsol system throughout a whole year (Cornu et al., 1998). The results showed that the precipitation input were negligible with regard to mineral-solution equilibrium in soil horizons. Mean concentrations and standard deviation in openfall were 0.02 ± 0.01, 0.03 ± 0.02 and $0.04 \pm 0.02\,\mathrm{mg\,l^{-1}}$ for dissolved Si, Al and Fe, respectively, in throughfall they were 0.08 ± 0.04, 0.06 ± 0.04 and $0.07 \pm 0.05\,\mathrm{mg\,l^{-1}}$, respectively. Stemflow fluxes were insignificant.

Regarding groundwater, thirteen zero-tension lysimeters were installed inside drilling holes at different depths, 2 points (CA2-20 and CA1-150) within the podzolic campinarana area (Fig. 1) and 11 points along the soil catena (Fig. 2). After installing the lysimeters, each drilling hole was tamped by filling with the previously extracted soil

BGD
9, 2233–2276, 2012

material at the corresponding depth. Each lysimeter was made of a 50 ml polypropylene bottle bored with 5 mm diameter holes all around. A 2 mm diameter capillary PTFE tube was inserted through the bottle cap in order to permit extracting water from the topsoil with a manual vacuum pump. To prevent clogging of the capillary tube by soil particles, a cylindrical filter made of a SeFar Nitex 64 µm polyamide open mesh was put inside the bottle. All lysimeters were acid-washed prior to installation.

The sampling points were selected with the purpose of identifying the main biogeochemical compartments of the soil system. The "CA2-20" point was situated at 20 cm depth in the podzolic campinarana area. It allowed sampling the upper part of the water-table circulating in the sandy podzol horizons, when the water-table was in high-level conditions and attained the A horizons. The "Spring" point was situated at the very beginning of a spring flowing from the center of the podzolic campinarana area. The spring always flowed during the sampling periods, with higher outflow immediately after rains. The samples corresponded thus to the upper part of the water-table circulating in the sandy podzol horizons. The "CA1-150" point was situated 150 cm in depth within the white sand E horizon, 50 cm over the Bh horizon; the "P4-240" point was situated at 240 cm in depth in the sandy-clay Bhs horizon. These two points allowed sampling the lower part of the water table perched over the Bhs horizons. The remaining sampling points were chosen in order to obtain a sequence of samples describing the lateral downslope flows along the studied catena.

2.2.2 Sampling and analysis

Groundwater was sampled during three periods indicated on Fig. 4. The first one (27 to 30 July 2007) was the drier, characterized by rains below the average of the period. The second one (29 January to 4 February 2008) was chosen in order to get low-level water-tables, the rains were however higher than the average of the season. The third period (19 to 25 May 2008) was chosen in order to get high-level water-tables and was actually the wetter period. The 10-days cumulated rainfalls before the sampling periods were 53, 88 and 178 mm for the 1st, 2nd and 3rd sampling periods,

BGD
9, 2233–2276, 2012

respectively. Complementary sampling for acid-base microtitration was realized on 9 February 2009 for points Spring, CA1-150, P4-240, P12-380 and P6-400.

Sampling was done by applying a continuous suction of 25 mmHg to the lysimeters. The first 20 ml of each sampling was discarded in order to avoid dead volume and to rinse the sampling equipment. Groundwater was then sampled until 250 ml was reached or air was entering the system. pH and E_H were measured immediately after sampling with a Eutech pH310 instrument after stabilization with gentle shake (calibration of the pH electrode was done every day). Each sample was then filtered using an inline 0.22 µm cellulose membrane filter (Nalgene surfactant-free cellulose acetate) and separated in four aliquots for immediate analysis of dissolved H_4SiO_4, Al^{3+}, Fe^{2+} and Fe^{3+}. A fifth aliquot was filtered using a 0.7 µm fiber glass filter, poisoned with sodium azide, stored in 10 ml vacuum glass flasks (Vacutainer) then kept at low temperature (around 4 °C) for laboratory analysis.

Analysis of dissolved H_4SiO_4, Al^{3+} and Fe^{2+}/Fe^{3+} were performed within one hour after sampling by colorimetry using a Lange DR 2800 Spectrophotometer with analytical kits LCK301, LCW028 and LCK320, respectively. The measurement ranges were 0.01–0.60 mg l^{-1}, 0.005–1.000 mg l^{-1} and 0.05–6.0 mg l^{-1} for Al^{3+}, H_4SiO_4 and Fe^{2+}, respectively. The colorimetric method was chosen because it allowed measurements immediately after sampling and because it measures the free or displaceable species able to participate to solution-minerals equilibria. To ensure that no oxidation of Fe^{2+} was occurring between sampling and analysis, Fe^{2+} measurements were performed 10 min and 6 h after water sampling. No significant differences between the results were observed. In order to limit possible interferences due to the natural color of the samples, mainly due to DOM, absorbance of the filtered sample before any reagent addition was subtracted from absorbance of the final measurement.

In the laboratory, DOC analyses were performed with a Shimadzu TOC-V Analyzer equipment calibrated with a 10 ppm potassium phthalate standard solution. Blank signal for ultra pure MQ water was about 0.1 ppm. Na^+, NH_4^+, K^+, Mg^{2+}, Ca^{2+}, F^-, Cl^-, NO_2^-, NO_3^-, PO_4^{2-}, SO_4^{2-} ions were determined by ion chromatography (Dionex DX

BGD
9, 2233–2276, 2012

120), using 9 mmol l^{-1} $NaHCO_3$ for cation elution and 10 mmol l^{-1} methane sulfonic acid for anion elution.

Some authors (Menzies et al., 1992) observed that colorimetric methods discriminate against micro-particulates but do not measure all Al present as soluble organic forms and thus underestimate total soluble Al. In order to check if some metal species were so strongly bonded to DOM that they were not displaced during the in-site colorimetric analysis, Al^{3+}, Fe^{2+} and Fe^{3+} were measured for a selected set of samples, before and after UV-oxidation of the DOM. Oxidation was performed in cylindrical quartz vessels using a 450 Watt Hanovia medium-pressure mercury lamp; complete DOM oxidation was checked by DOC determination after irradiation. Results gave no significant differences in concentrations before and after UV-oxidation of the DOM, so that we may conclude that the colorimetric method gave the sum of free plus OM-bonded species for Al and Fe.

During data modeling, the pH values seemed underestimated in comparison to field observations, so that a special attention was paid to pH measurements. pH electrode calibration at field was realized with a standard electrode and standard reference solutions having a ionic strength high when compared to the studied solutions, which can give a measurements error. To test this hypothesis, pH measurement were achieved on seven selected samples, using the same electrode and adjusting the ionic strength (I) to 10^{-4}, 10^{-3} and 10^{-2} M with KCl. The pH increased with increasing ionic strength, an asymptote being reached when $I = 10^{-2}$ M (Supplement, Fig. S1). The difference ΔpH between pH measured before adjustment and pH measured at $I = 10^{-2}$ M was depending on the DOC content, which indicates that the DOM is actually charged and participates to the ionic strength. The pH were then corrected by using the empirical relationship [ΔpH = 0.508–0.0047 × DOC] where DOC is expressed in mg l^{-1}.

In order to evaluate the behaviour of the studied solutions with regard to H^+, acid-base logarithmic scale microtitrations of selected samples were performed with 0.2 mol l^{-1} HNO_3 and 0.1 mol l^{-1} KOH, using two Titrino 719 apparatus controlled by a Tinet 2.4 software.

BGD
9, 2233–2276, 2012

Thermodynamic modeling of the solution-minerals interactions was performed by own calculation and checked using the PHREEQ-C (2.11) software with the Wateq-4f database (Ball and Nordstrom, 1991).

3 Results

3.1 Water pathways along the catena

During the 1st sampling period, no samples were available in the P13-160 and P12-160 points, because of the lack of perched water-table in the Ef horizon due to insufficient rainfall. During the 2dn sampling period, the point P13-160 gave sample only one sampling day (31/01/08) when the P12-160 point gave sample three sampling days (29/01/08, 31/01/08 and 02/02/08). During the 3rd sampling period, both P13-160 and P12-160 points gave samples every sampling day. This behaviour of the sampling points attests the fast level changes of the perched water table after heavy rains. When sufficiently high, a water table perched over the podzolic Bhs horizon laterally overflows towards the Ef horizon, then percolates downslope along this horizon or flows out in the flat-bottomed micro-valleys. Considering the point PMVB-15, the waters sampled during the 1st sampling period came necessarily from recent rainfall percolating the topsoil horizons, because of the lack of perched water table, when during the 2nd and 3rd sampling the waters could come from both recent rainfalls percolating topsoil horizons and overflowing of the perched water table. Excepting point P12-380 and downslope point P24-80, other sampling points of the catena gave samples every sampling day.

Two water pathways can thus be defined along the catena (Fig. 2). A deep, permanent water table flows more than two meters deep within the kaolin horizons. The lateral flow of its upper part corresponds to pathway no. 1 and is described by the following succession of samples: P4-510 – P13-490 – P12-380 – P6-400 – P23-380 – P24-300. A temporary, closer to the surface water table circulates in the Es and Ef horizons only after heavy rainfalls and can overflow in the micro-valleys. It corresponds

BGD
9, 2233–2276, 2012

to pathway no. 2 and is described by the following succession of samples: P4-240 – P13-160 – P12-160. The PMVB-15 point was situated at the bottom of a small micro-valley, at an altitude roughly corresponding to those of the P13-160 point, and allowed sampling the overflow of the perched water-table in the micro-valleys. Such overflow allows a direct exportation of the groundwater down to the streams and rivers, beside other pathways such as the usual overflowing of the groundwater in the lower parts of the landscape or pipes as observed elsewhere (Lucas et al., 1996).

3.2 Composition of the percolating waters

The composition of the groundwater from each sampling point and for each sampling day for dissolved Si, Al^{3+}, Fe^{2+}, Fe^{3+}, pH, E_H and DOC is given in the Supplement; Table S1 and statistics from these data are given in Table 2. Some key points, representing the different kinds of circulating waters (Spring, CA2-20, CA1-150, P4-240, P4-510, P13-490, P6-400 and P24-300), were chosen for analysing other solutes (Na^+, NH_4^+, K^+, Mg^{2+}, Ca^{2+}, Cl^-, NO_2^-, NO_3^-, SO_4^{2-}, S^{2-} and F^-). Results are given in Table 3, except for S^{2-} and F^- which remained negligible.

For most sampling points, the chemistry of the collected waters showed low variations within a sampling period as well as between sampling periods, an example is given on Fig. 5 (P4-240 and P4-510 sampling points). This assessed the coherence and the overall quality of the obtained data. The results are hereafter described and discussed following the two pathways of the circulating waters, pathway no. 1 for the deep water-table and pathway no. 2 for the perched water table. Average compositions of circulating waters by sampling periods and overall averages are given in Fig. 6 for pathway no. 1 and Fig. 7 for pathway no. 2. The first sampling period is not given for pathway 2 because the Ef horizon lacked free water at this period. For each pathway, there is a very good similarity of the changes in the water chemistry between one sampling day to the other and between the three sampling periods (Fig. 6a–c). It is thus pertinent to comment the water chemistry changes from the overall average (Figs. 6d and 7c) for an easier understanding.

BGD
9, 2233–2276, 2012

3.2.1 From the podzolic sands downslope following the deep water table (pathway no. 1)

pH

The pH was acidic for all samples, ranging from 3.4 to 5.5. The minimum values were observed for the waters circulating in the white sand (points CA2-20 and CA1-150) and in the underlying Bhs (point P4-240). Those waters were also the more acidic on the average (4.1), and their maximum values did not exceeded 4.5. Regarding the deep water table, the pH progressively increased downslope from point P4-510 (average 4.5) to point P24-300 (average 5.0). The pH slightly changed from one sampling period to the other, but considering each sampling period individually, the pH increase in the downslope direction was always progressive and significant (Fig. 6a–c). pH values over 5.2 were only observed for the three points situated at the lower part of the slope (P6-400, P23-380, P24-300).

DOC concentrations

The waters from the upper horizons of the podzolic area (CA2-20) had high DOC concentrations; the averages were 46, 36 and 27 $mg\,l^{-1}$ for the 1st, 2nd and 3rd periods, respectively. The diminution from a period to the other was likely a dilution effect due to higher rainfall. The water sampled at 150 cm in depth in the white sand (CA1-150) had a more buffered composition throughout the three periods (37, 37 and 43 $mg\,l^{-1}$, respectively). In the Bhs horizon (P4-240), the DOC concentration varied from 12 to 19 $mg\,l^{-1}$, 15 $mg\,l^{-1}$ on average. In the deep clayed horizons (points P4-510 to P24-300), the DOC concentrations were lower but no negligible, varying from 1.5 to 9.7 $mg\,l^{-1}$, 4.0 $mg\,l^{-1}$ on average, without significant variations along the catena.

BGD
9, 2233–2276, 2012

Si and Al concentrations

The waters from the upper horizons of the podzolic area (CA2-20) had always very low Si and Al concentrations. The maximum values for Si and Al were 0.1 and 0.14 mg l^{-1}, respectively, and the average values were 0.05 and 0.03 mg l^{-1}, respectively. On the other hand, the waters from the Bhs horizon (point P4-240) had the highest Si and Al values observed during the three sampling periods: Si ranged from 0.29 to 0.59 mg l^{-1} and Al ranged from 0.37 to 0.63 mg l^{-1}. At every sampling day the Si and Al values were close together (Fig. 5) and their averages over the three sampling periods were 0.48 mg l^{-1} for both. The waters from point CA1-150 had values intermediate between those of points CA2-20 and P4-240. From the Bhs horizon down to the kaolin horizon, i.e. from point P4-240 to point P4-510, the Si concentrations underwent a strong decrease, down to 0.13 mg l^{-1} on average, when the Al values suffered a slighter decrease, down to 0.37 mg l^{-1} on average. Going downslope, from point P4-510 to point P24-300, the Si values progressively increased again up to values around 0.5 mg l^{-1}, when the Al values continued a progressive decrease, down to values most time under the detection limit on point P23-380, then increased slightly on the last point (P24-300).

Fe concentrations and E_H

For all points except P12-380, Fe^{2+} concentrations were higher than Fe^{3+} concentrations. The Fe^{3+} and Fe^{2+} concentrations exhibited, however, a close behaviour along the whole catena except the last downslope point, i.e. from point CA2-20 to point P23-380. For these points, Fe^{3+} and Fe^{2+} concentrations were frequently below the quantification limit and no individual samplings exceeded 0.20 and 0.46 mg l^{-1} for Fe^{3+} and Fe^{2+}, respectively. The points situated upslope in the white sand (CA2-20 and CA1-150) and in the Bhs horizon (P4-240) had values more variable and higher than the points situated midslope in the deep kaolin (P13-490 to P6-400). Those Fe^{3+} and Fe^{2+} values corresponded to E_H values varying from 410 to 575 mV, without significant correlation between these variables. Downslope, the behaviours of Fe^{3+} and

BGD
9, 2233–2276, 2012

Fe^{2+} concentrations diverged: when the Fe^{3+} concentrations remained low, the Fe^{2+} concentrations increased slightly on point P23-380 then drastically on point P24-300 with a 0.57 mg l^{-1} average value. The increase of the Fe^{2+} concentrations on the last downslope point is closely related to a decrease of the E_H. The E_H remained between 410 and 575 mV along the whole catena excepting the last downslope point were it was between 209 and 253 mV.

The waters from the Spring point had pH and chemical characteristics very similar to those observed for the CA2-20 point, except regarding the E_H which was higher (521 ± 15 versus 473 ± 17 mV).

3.2.2 From the podzolic sands downslope following the perched water table (pathway no. 2)

pH and DOC concentrations

The transition from the point P4-240 to the points P13-160 then P12-160 came with a pH increase between 0.5 to 1 pH unit (4.1, 4.6 and 4.9 on average, respectively) and a progressive decrease of the DOC concentrations, from 15 to 5 then 4 mg l^{-1} on average, respectively. The point PMVB-15 had pH values similar to those of points P13-160 and P12-160 (4.6 on average), but DOC values always higher than 27 mg l^{-1} (32 mg l^{-1} on average).

Si and Al concentrations

The Si concentrations remained the same or most time slightly increased when passing from point P4-240 (average 0.48 mg l^{-1}) to point P13-160 (average 0.46 mg l^{-1}), then decreased markedly on point P12-160 (average 0.30 mg l^{-1}). Al concentrations had a decrease already marked on point P13-160 (average 0.20 mg l^{-1} versus 0.48 on point P4-240) and continuing on point P12-160 (average 0.06 mg l^{-1}). The different behaviour of Si and Al resulted in a progressive increase of the Si/Al molar ratio based

BGD
9, 2233–2276, 2012

on average values: 1.0 at point P4-240, 2.3 at point P13-160 and 4.8 at point P12-160. The waters sampled from point PMVB-15 were characterized by high Si and Al concentrations when compared to the other sampling points, on the average 1.86 and 0.68 mg l^{-1} for Si and Al, respectively, with a Si/Al molar ratio varying between 1.8 and 4.1 (2.7 for the average of ratios).

Fe^{2+}, Fe^{3+} concentrations and E_H

The Fe^{2+} concentrations increased when passing from point P4-240 (0.10 mg l^{-1} on average) to point P13-160 (0.21 mg l^{-1} on average) (excepting on the 19/05/08), then decreased on point P12-160 (0.05 mg l^{-1} on average). The Fe^{2+} concentrations on point P13-160 exhibited, however, a high variability, with a standard deviation (0.24) higher than the average value. The high Fe^{2+} concentrations were always related to lower E_H values, which reflects on the average values of E_H: 501, 399 and 482 mV for points P4-240, P13-160 and P12-160, respectively. There is no, however, a good correlation coefficient between the bulk of Fe^{2+} and E_H values. The Fe^{3+} concentrations remained always lower than 0.08 mg l^{-1} for both P13-160 and P12-160 points. The waters sampled at point PMVB-15 had high Fe^{2+} and Fe^{3+} concentrations (on average 1.58 and 0.79 mg l^{-1}, respectively) when compared to any other sampling point, and relatively low E_H values (372 mV on average).

3.3 Microtitration of Soil Solutions

Microtitrations were achieved on solutions sampled on 25 May 2008 from the Spring and CA1-150 points; an example of microtitration curve is given on Fig. 8. Three repetitions were made for each sample. The acid-base properties of the DOC were evaluated by fitting these results with the PROSECE software (Garnier et al., 2004a, b). This model consider a discrete distribution of acidic sites whose acidic constants pKa_i and site densities $L_{T,i}$ are determined by fitting the experimental curves. Here we chose 4 acidic sites, a sufficient number to ensure a good fitting of the experimental curves.

BGD
9, 2233–2276, 2012

The results are given on Table 4. The total calculated site densities were 40.2 ± 6.1 and 27.2 ± 3.6 meq gC^{-1} for the Spring and the CA1-150 samples, respectively.

4 Discussion

4.1 Evolution of the percolating waters along the Catena

4.1.1 Waters in the Podzolic Area

The spring water and the water circulating in the upper part of the white sands (CA-020 point) had similar characteristics: the highest DOC and the lower pH and Si values compared to all other samples and very low Al, Fe^{2+} and Fe^{3+} values (0.05, 0.02 and lower than 0.01 mg l^{-1} on average for dissolved Si, Al and Fe, respectively). These values are in the range of values observed by Cornu et al. (1997, 1998) in a similar podzolic area – same soil and vegetation – situated near Manaus. Dissolved Si, Al and Fe found here can come from canopy leaching, litter mineralization and dissolution of quartz and trace minerals (Table 2).

Compared to these waters, the water circulating in the lower part of the white sand and within the Bhs (CA1-150 and P4-240, respectively) had higher concentrations in Si, Al and Fe, which can be related to the proximity of the underlying kaolin horizon. The water circulating in the white sand horizons is quite aggressive with regard to clay or iron minerals, due to its acidity and to the complexing capacity of the DOC. The dissolution of kaolinite and Fe-oxides at the transition between white sands and kaolin horizon, in the Bhs horizons, is thus able to increase the water concentrations for Si, Al and Fe. Up and down movements of water due to the fluctuations of the water-table favour the dispersion of these solutes in the perched water-table, where concentrations should be higher when closer to the Bhs horizons, what was observed when comparing a point situated 50 cm over the Bh (CA1-150) and a point within the Bhs (P4-240). The molar values of dissolved Si and Al at point P4-240 were very close one to the other

BGD
9, 2233–2276, 2012

(1.7×10^{-5} and 1.8×10^{-5} mol l^{-1} for Si and Al, respectively), which is coherent with the hypothesis of a congruent dissolution of kaolinite in the Bhs horizons. The diminution of DOC concentration when water passes from the white sand to the Bhs is due to the DOC adsorption on kaolinite or Fe-oxides and gibbsite surfaces (Davis, 1982; Kaiser and Zech, 2000; Bardy et al., 2008; Fritsch et al., 2009).

4.1.2 Waters in the kaolin horizons (pathway no. 1)

Passing from the Bhs (point P4-240) to the underlying deep kaolin (point P4-510), the water suffered a slight pH increase, a drastic decrease of DOC, a decrease of Si and a slight decrease of Al and Fe. The DOC decrease is explained by adsorption of humic substances on clay and Fe mineral surfaces. The water percolating in the deep kaolin horizons, however, kept up a significant concentration of a specific DOC that did not adsorbed on clay surfaces.

Si, Al and Fe variations in percolating waters as well as the higher content of gibbsite and Fe-oxides at the upper part of the kaolin horizons can be explained by the following considerations. The DOM which migrates through the sandy horizons is carrying complexed Al and Fe. Most organo-metallic complexes adsorb on mineral surfaces in the Bh-Bhs, but do not accumulate indefinitely and most of them will eventually be mineralized, releasing Al and Fe in the soil solution. Fe precipitates as Fe-oxides (likely goethite and lepidocrocite) and Al precipitates as kaolinite, resulting in the decrease of Si concentration. Al in excess precipitates as gibbsite, giving high gibbsite content in the horizons immediately beneath the Bhs (Fig. 3).

Going downslope in the deep kaolin horizons, following the sample points sequence P4-510, P13-490, P12-380, P6-400, P24-300, the progressive pH increase is more related to a progressive increase of the sum of charges of major ions than to a diminution of the charges due to the DOM (Table 5). The increase of Na^+, K^+, Ca^{2+} and Mg^{2+} concentrations when going downslope is likely due to higher content in weatherable minerals closer to the soil surface. The pH increase could explain the precipitation of

BGD
9, 2233–2276, 2012

Al as gibbsite nodules (Fig. 2) and the consecutive decrease of Al concentration in the soil solution (Fig. 6).

4.2 Waters in the perched water table (pathway no. 2)

When flowing from the white sand to the non-podzolic leached horizon Ef, passing the Bhs, the groundwater loosed most of its DOC, but remained with relatively high DOC concentrations. Such water remains aggressive with regard to secondary minerals and can favour the clay impoverishment of the Ef horizon with a positive feedback. The increase of the Si/Al molar ratio is explained by precipitation of Al as gibbsite as observed downslope along the pathway no. 1. In the micro-valley bottom, at point PMVB-15, Si, Al and Fe values are exceptionally high with regard to the high rainfall climate; Si values for example may approach the quartz solubility (2.9 mg l^{-1}). This may be due to the fact that the water sampled at this point added dissolved elements brought by the overflowing groundwater and elements locally produced by the litter degradation.

4.3 The properties of the dissolved organic matter

Table 5 reports the ion balance for the samples given on Table 3. The remaining negative charge due to the DOM (Z_{DOM}) expressed in meq C^{-1} was calculated from the sum of charges of major ions expressed in µeq l^{-1}, the pH and the dissolved organic carbon concentration expressed in mg l^{-1}, using the following equation:

$$Z_{DOM} = \frac{\left(10^{-6pH} - \sum_i Z_i\right)}{COD} \quad (1)$$

The average DOM charge ranged from −6.2 to −6.5 meq gC^{-1} for the water circulating in the sandy podzol horizons, was −11 meq gC^{-1} for the water in the deep Bhs and ranged from −31 to −37 meq gC^{-1} for the waters circulating in the deep Bhs and in the

BGD
9, 2233–2276, 2012

deep kaolinitic horizons. The DOM circulating in the kaolinitic horizons had therefore values much higher than the DOM from the white sands. As all the waters were quite acidic, most of the charges were due to carboxylic-type sites. With the aim to give an order of magnitude, the acid site density L_T expressed in meq gC^{-1} was modelled for a single carboxylic-type ligand, considering various pKa from 3 to 4.5, using the following equation:

$$L_T = Z_{DOM}\left(1 + 10^{pKa-pH}\right) \quad (2)$$

The results are given on Table 5. The calculated acid-site densities of the DOM circulating in the white sands horizons range from 7 to 23 meq gC^{-1} when considering a pKa ranging from 3 to 4.5. This is consistent with the values obtained by modelling the microtitration curves for the Spring and CA1-150 points (26.7 ± 0.8 and 18.0 ± 0.8 meq gC^{-1} for carboxylic-type sites, respectively). Regarding carboxylic-type acid site densities, we found no data for equatorial podzols or ferralsol groundwater available in the literature. In comparison, Ravichandran et al. (1998) obtained a total of acid-site densities ranging from 1.45 to 3.8 meq gC^{-1} for various humic substances (AF and AH) coming from the Everglades and from Suwanee River, i.e. lower values than reported here. Considering natural waters, total carboxylic acid site density obtained in pristine boreal areas (Köhler et al., 1999; Cuss et al., 2010) or springs from acid podzolic temperate zone (Hruska et al., 2003) were 8.6 ± 1.6, 9.8 ± 0.24 and 10.2 ± 0.6 meq gC^{-1}, respectively. These values are in the range of those reported here.

The DOM circulating in depth in the kaolinitic horizons was quite different. Considering a pKa ranging from to 3 or 4.5, the calculated site densities are quite high, ranging from 31 to 67 meq gC^{-1} (in comparison, one site per carbon would give a site density equal to 83.3 meq gC^{-1}). This DOM has thus likely a high proportion of small carboxylic acids such as formic, oxalic or citric acids whose site densities are 83.3, 83.3 and 41.7 meq gC^{-1}, respectively. The ability of such small carboxylic compounds to percolate through a kaolinitic material can be explained by the fact that they are more

BGD
9, 2233–2276, 2012

hydrophilic than larger, humified components usually hydrophobic. It is also coherent with results obtained by Kang and Xing (2007), which showed that the adsorption of carboxylic acids on clay surfaces is lower when the compounds are small and is lower on kaolinite than on 2:1 clays. Kaiser and Zech (2000) showed that the sorption of DOM on the clay fraction is sharply reduced when Fe-oxides and gibbsite are removed from the clay fraction. Indeed, the Fe-oxides and gibbsite contents are very low in the white kaolin horizon. When the solutions percolating in the white kaolin reach a material with a higher content in Fe-oxides and gibbsite, the DOM can be adsorbed, then mineralized, resulting in the release of previously DOM-complexed Al or Fe and a positive feedback for Fe-oxides and gibbsite. This specific DOM which circulates in the kaolinitic horizons can be a fraction of the DOM which circulates in the white sands or be produced by microbial activity in the Bh-Bhs.

4.4 Groundwater – minerals relationships

4.4.1 The Si-Al system

The positions of the average groundwaters in the Si-Al system are given in Fig. 9. The line "kaolinite 1" corresponds to the stability with kaolinite calculated with the Wateq-4f data base, which uses the same value ($\log(K_{sp}) = 3.705$) than the one proposed by Tardy and Nahon (1985) after a critical analysis of the literature. However, as stressed by Grimaldi et al. (2004), kaolinite solubility is not well defined in most tropical soils because of iron substitution and variable crystallinity and these authors also used a lower value ($\log(K_{sp}) = 2.853$) that gave the line "kaolinite 2" in Fig. 9.

The relative positions of the points are consistent with the evolution of the groundwater along the slope as discussed above.

Even without considering complexation by DOM, the spring water and the groundwater circulating in upper part of the white sands (Spring and CA2-20) are far away from saturation with kaolinite or gibbsite. Excepting point P23-380, the groundwaters circulating in the kaolinitic horizons (from P4-510 to P24-300 along the pathway no. 1

BGD
9, 2233–2276, 2012

and from P12-160 to P13-160 along the pathway no. 2) are all close to the "kaolinite 1" line, which indicates a control by kaolinite precipitation/dissolution. Their evolution downslope (white arrow), i.e. which increasing residence time, is thus driven by an increase of Si concentrations likely due to quartz dissolution. Most are supersaturated with regard to gibbsite, which is consistent with gibbsite precipitation in slope horizons (see envelope of centimetrical Al-nodules on Fig. 2) but may also indicate a higher gibbsite solubility or Al complexation with DOM. No explanation was found for the fact that the point P23-380 is far away from equilibrium due to the very low Al concentrations that have always been observed along the three sampling periods, although these low values are consistent with the gradual decrease of Al concentration in the groundwater along the slope. The micro-valley bottom groundwater (PMVB-15) is clearly oversaturated with regard to kaolinite because of very high Si concentrations likely due, as stressed before, to litter mineralization.

Complexation by DOM was roughly calculated using a complexation constant between DOM and Al equal to 10^5 and a site density extrapolated from Table 5 for pKa = 3. When considering complexation by DOM, all points are far away from equilibrium with gibbsite or kaolinite. A correct modelling of the role of organic matter, however, would require a better understanding of the complexation properties of the DOM relative to Al, Fe and other dissolved species; this will be the subject of a further publication.

4.4.2 Iron, iron bearing minerals and bleaching of the kaolin

Measured Fe^{2+} values were almost always higher than Fe^{3+} values, indicating that iron in the soil system is mainly transported as Fe^{2+} even when E_H is relatively high, more than 450 mV. As seen in the Fe Pourbaix diagram (Fig. 10), the DOM-rich groundwaters from the white sands or the micro-valley bottom (circles) are well below the Fe^{2+}/Fe^{3+} transition, which is explained by acidity for the white-sand groundwater and by lower E_H for micro-valley bottom (PMVB-15) where litter mineralization occurs. Excepting the P13-160 point, all DOM-poor groundwaters circulating in the kaolin as well as in the Ef horizons are close to the Fe^{2+}/Fe^{3+} transition, most time slightly below,

BGD
9, 2233–2276, 2012

indicating that the mobility of iron in theses horizons depends on small E_H variations which can be due to microbial pulses in upper horizons or Bh-Bhs organic matter mineralization (Montes et al., 2007). According to Cornell and Schwertmann (1996), the bright orange-coloured coatings in tubular pores observed immediately beneath the Bhs are characteristics of lepidocrocite, which forms by fast iron precipitation in soils submitted to rapid E_H changes. The position of the P13-160 point (Ef horizon) is characterized by a low E_H when compared to the upstream P4-240 or CA1-150 points or the downstream P12-160 point. This may be due to the fact that the water sampled at this point has just flowed through the Bh-Bhs where organic matter oxidation may lower the E_H. Downslope, sulphide-smelling groundwaters of point P24-300 are typical of reduced conditions.

Considering the obtained results, two processes are able to favour the bleaching of the kaolin associated with podzols areas. The first one, as hypothesized by Montes et al. (2007), is that solutions percolating in depth are able to reduce iron and that their reducing capacity can be enhanced by mineralization in depth of the organic matter transferred from the topsoil by podzolic processes. The second one is that, because of the podzolic conditions in the topsoil, the incomplete mineralization of organic matter results in the production of a DOM rich in carboxylic coumpounds which are transferred down to the deep Bh-Bhs. A part of the these coumpounds – most of them small, highly carboxylic – are able to pass through the Bh-Bhs and to migrate within the kaolin, enhancing the iron mobility by complexing Fe^{3+} and, as already observed in very oxidizing media (Kieber et al., 2005), Fe^{2+}. The final result is a complete bleaching of kaolin horizons and it is likely that the deeper the permanent water-table, the thicker the kaolin bleached horizons.

5 Conclusions

The compositions of the groundwaters percolating the soil system are consistent with the observed mineral and organic paragenesis, which indicates that these paragenesis

BGD
9, 2233–2276, 2012

are produced under the current climate and change spatially according to the dynamics of the soil system.

The groundwater circulating in the podzol *E* white sand horizons is acidic, around pH 4.1, and has a high DOC content, around 37 mg l^{-1}. The acid-site density of its DOM ranges from 7 to 23 meq gC^{-1}, considering pKa's between 3 and 4.5; these properties are similar to those observed in podzolic temperate areas. The aggressiveness of such a solution with regard to secondary minerals favours the podzol development at the expense of the ferralsolic or kaolin material, which is in accordance with the system dynamics inferred from soil horizons morphology (Lucas et al., 1996). The black waters of the river system originate from the white-sand groundwater, which seeps and overflows in the lower parts of the podzolic areas and can also, after high rainfall events, drain through a specific network of micro-valleys at the podzol-ferralsol transition.

Part of the white sand, DOM-rich groundwater percolates in depth and reach horizons having clay or Fe-oxides. Most of the DOM then adsorbs on mineral surfaces, forming Bh-Bhs horizons. The turn-over of this adsorbed organic matter results in the release of previously complexed Al and Fe, which can precipitate within the lower part of the Bhs and in the upper meter of the kaolin. Some DOM is, however, able to percolate through clayey materials at significant concentrations, up to 9 mgC l^{-1}. This specific DOM has quite high site densities, ranging from 31 to 67 meq gC^{-1} when considering a pKa ranging from 3 to 4.5, indicating a large proportion of small carboxylic acids.

In the deep kaolin and in the ferralsolic horizons, the Si and Al content of the groundwater is controlled by gibbsite and kaolinite precipitation/dissolution and by quartz dissolution. Fe is mainly transported as Fe^{2+}, due to acidity and relatively low E_H; its mobility is related to small E_H variations for which microbial activity can be decisive. Fe and Al species mobility is also enhanced by the significant concentration of the small carboxylic acids directly related to the podzolic processes occurring upflow. The long-term result of these processes is the bleaching of the kaolin, the precipitation of Al-nodules in slope horizons and of Fe-oxides in the upper downslope horizons. An

BGD
9, 2233–2276, 2012

accurate modelling of the minerals-solutions relationships will, however, need further investigation of the DOM acidity and complexing properties with regard Al and Fe.

As bleaching of the kaolin is favoured by the deep percolation of white-sand issued solutions, it is likely that thick bleached kaolin can be found everywhere presently active giant podzols are close to a slope gradient sufficient to lower the water-table.

With regard to methods, it must be noticed that usual pH measurement protocols are inadequate for low ionic strength groundwaters and that pH measurement must be adapted by using low ionic strength references, by adjusting the ionic strength during pH measurement or by using a corrective model.

Supplementary material related to this article is available online at: http://www.biogeosciences-discuss.net/9/2233/2012/bgd-9-2233-2012-supplement.zip.

Acknowledgements. This work benefited from FAPESP funding no. 07/02543-0, from ARCUS PACA-Brésil funding (French Ministry of Foreign Affairs MAE and Région Provence-Alpes-Côte d'Azur) and from CAPES-COFECUB bilateral cooperation funding.

References

Ball, J. W. and Nordstrom, D. K.: User's manual for Wateq4F, with revised thermodynamic data base and test cases for calculating speciation of major, trace, and redox in natural waters, US Geol. Survey Open File Rep., 91–183, 1991.

Bardy, M., Fritsch, E., Derenne, S., Allard, T., do Nascimento, N. R., and Bueno, G. T.: Micro-morphology and spectroscopic characteristics of organic matter in waterlogged podzols of the upper Amazon basin, Geoderma, 145, 222–230, 2008.

Batjes, N. H. and Dijkshoorn, J. A.: Carbon and nitrogen stocks in the soils of the Amazon Region, Geoderma, 89, 273–286, 1999.

Benedetti, M. F., Ranville, J. F., Allard, T., Bednar, A. J., and Menguy, N.: The iron status in colloidal matter from the Rio Negro, Brasil. Coll. Surf. A., 217, 1–9, 2003.

BGD
9, 2233–2276, 2012

Bernoux, M., Carvalho, M. C. S., Volkoff, B., and Cerri, C. C.: Brazil's soil carbon stocks, Soil Sci. Soc. Am. J. 66, 888–896, 2002.
Boulet, R., Chauvel, A., Humbel, F. X., and Lucas, Y.: Analyse structurale et cartographie en pédologie I: Prise en compte de l'organisation bidimensionnelle de la couverture pédologique: les études de toposéquences et leurs principaux apports à la connaissance des sols, Cah. ORSTOM, sér. Pédol. XIX, 4, 309–321, 1982.
Bravard, S. and Righi, D.: Characterization of fulvic and humic acids from an Oxisol-Spodosol toposequence of Amazonia, Brazil, Geoderma, 48, 151–162, 1991.
Chauvel, A., Lucas, Y., and Boulet, R.: On the genesis of the soil mantle of the region of Manaus, Central Amazonia, Brazil, Experientia 43, 234–241, 1987.
Chauvel, A., Walker, I., and Lucas, Y.: Sedimentation and pedogenesis in a Central Amazonian Black water basin, Biogeochemistry, 33, 77–95, 1996.
Cornell, R. M. and Schwertmann, U.: The Iron Oxides: Structure, Properties, Reactions and Uses, VCH, Weinheim, 1996.
Cornu, S., Ambrosi, J. P., Lucas, Y., and Fevrier, D.: A comparative study of the soil solution chemistry of two Amazonian forest soils (Central Amazonia, Brazil), Hydrol. Earth Syst. Sci., 1, 313–324, doi:10.5194/hess-1-313-1997, 1997.
Cornu, S., Lucas, Y., Ambrosi, J. P., and Desjardins, T.: Transfer of dissolved Al, Fe and Si in two amazonian forest environment in Brazil, Eur. J. Soil Sci., 49, 377–384, 1998.
Cuss, C. W., Guéguen, C., Hill, E., and Dillon, P. J.: Spatio-temporal variation in the characteristics of dissolved organic matter in the streams of boreal forests: Impacts on modelled copper speciation, Chemosphere, 80, 764–770, 2010.
Dall'Agnol, R. and Macambira, M. J. B.: Titanita-biotita granitos do baixo Rio Uaupés, Província Rio Negro, Amazonas – Parte 1: Geologia, petrografia e geocronologia, Rev. Bras. Geocienc., 22, 3–14, 1992.
Davis, J. A.: Adsorption of natural dissolved organic matter at the oxide/water interface, Geochim. Cosmochim. Ac., 46, 2381–2393, 1982.
Delarue, F., Cornu, S., Daroussin, J., Salvador-Blanes, S., Bourennane, H., Albéric, P., Vennink, A., Bruand, A., and King, D.: 3-D representation of soil distribution: An approach for understanding pedogenesis, C. R. Geosci., 341, 486–494, 2009.
Dubroeucq, D. and Volkoff, B.: From oxisols to spodosols and histosols: evolution of the soil mantles in the Rio Negro Basin (Amazonia), Catena, 32, 245–280, 1998.
Fritsch, E. and Fitzpatrick R. W.: Interpretation of soil features produced by ancient and modern

BGD
9, 2233–2276, 2012

processes in degraded landscapes – Part 1: A new method for constructing conceptual soil-water-landscape models, Aust. J. Soil Res. 32, 889–907, 1994.
Fritsch, E., Allard, T., Benedetti, M. F., Bardy, M., do Nascimento, N. R., Li, Y., and Calas, G.: Organic complexation and translocation of ferric iron in podzols of the Negro River watershed. Separation of secondary Fe species from Al species, Geochim. Cosmochim. Ac., 73, 1813–1825, 2009.
Garnier, C., Mounier, S., and Benaim, J. Y.: Influence of dissolved organic carbon content on modelling natural organic matter acid-base properties, Water Res., 38, 3685–3692, 2004a.
Garnier, C., Pizeta, I., Mounier, S., Benaim, J. Y., and Branica, M.: The influence of the type of titration and of data treatment method on metal complexing parameters determination of single and multi ligand systems measured by stripping voltammetry, Anal. Chim. Acta, 505, 263–275, 2004b.
Grimaldi, C., Grimaldi, M., Millet, A., Bariac, T., and Boulègue, J.: Behaviour of chemical solutes during a storm in a rainforested headwater catchment, Hydrol. Process., 18, 93–106, 2004.
Hruska, J., Köhler, S., Laudon, H., and Bishop, K.: Is a universal model of organic acidity possible: comparison of the acid/base properties of dissolved organic carbon in the boreal and temperate zones, Environ. Sci. Technol., 37, 1726–1730, 2003.
IBGE: Levantamento pedológico, folhas NA-19, NA-20, SA-19 e SA-20. CREN-IBGE, São Paulo, 2009.
Ishida, D. A.: Caracterização e gênese de solos e de depósito de caulim associado, São Gabriel da Cachoeira – AM, Thesis, Universidade de São Paulo, 172 pp., 2010.
Kaiser, K. and Zech, W.: Dissolved organic matter sorption by mineral constituents of subsoil clay fractions, J. Plant. Nutr. Soil Sci., 163, 531–535, 2000.
Kang, S. and Xing, B.: Adsorption of dicarboxylic acids by clay minerals as examined by in situ ATR-FTIR and ex situ DRIFT, Langmuir, 23, 7024–7031, 2007.
Kieber, R. J., Skrabal, S. A., Smith, B. J., and Willey, J. D.: Organic Complexation of Fe(II) and Its Impact on the Redox Cycling of Iron in Rain, Environ., Sci. Technol., 39, 1576–1583, 2005.
Köhler, S., Hruska, J., and Bishop, K.: Influence of organic acid site density on pH modeling of Swedish lakes, Can. J. Fisch Aquat. Sci., 56, 1461–1470, 1999.
Leenheer, J. A.: Origin and nature of the humic substances in the waters of the Amazon River basin, Acta Amazonica, 10, 513–526, 1980.
Lucas, Y., Chauve,l A., Boulet, R., Ranzani, G., and Scatolini, F.: Transiçâo latossolos-podzois

BGD
9, 2233–2276, 2012

sobre a formaçâo Barreias na regiâo de Manaus, Amazônia, Rev. Bras. Ci. Solo, 8, 325–335, 1984.
Lucas, Y., Boulet, R., and Chauvel, A.: Intervention simultanée des phénomènes d'enfoncement vertical et de transformation latérale dans la mise en place de systèmes de sols de la zone tropicale humide: Cas des systèmes sols ferrallitiques – podzols de l'Amazonie Brésilienne, C. R. Acad. Sci. Ser. II, 306, 1395–1400, 1988.
Lucas, Y., Luizão, F. J., Chauvel, A., Rouiller, J., and Nahon,, D.: The relation between biological activity of the rainforest and mineral composition of the soils, Science, 260, 521–523, 1993.
Lucas, Y., Nahon, D., Cornu, S., and Eyrolle, F.: Genèse et fonctionnement des sols en milieu équatorial, C. R. Acad. Sci. Ser. II, 322, 1–16, 1996.
Lundström, U. S., van Breemen, N., and Bain, D.: The podzolisation process, a review, Geoderma, 94, 91–107, 2000.
Menzies, N. W., Kerven, G. L., Bell, L. C., and Edwards, D. G.: Determination of total soluble aluminum in soil solution using pyrocatechol violet, lanthanum and iron to discriminate against micro-particulates and organic ligands, Com. Soil Sci. Plant. Anal., 23, 2525–2545, 1992.
Montes, C. R., Lucas, Y., Melfi, A. J., and Ishida, D. A.: Systèmes sols ferrallitiques-podzols et genèse des kaolins, C. R. Geosci., 339, 50–56, 2007.
Montes, C. R., Lucas, Y., Pereira, O. J. R., Achard, R., Grimaldi, M., and Melfi, A. J.: Deep plant-derived carbon storage in Amazonian podzols, Biogeosciences, 8, 113–120, doi:10.5194/bg-8-113-2011, 2011.
Munsell: Munsell soil color chart, Kollmorgen Instruments Corp., New York, 1990.
Nascimento, N. R., Bueno, G. T., Fritsch, E., Herbillon, A. J., Allard, T., Melf,i A., Astolfo, R., Boucher, H., and Li, Y.: Podzolization as a deferralitization process: a study of an Acrisol-Podzol sequence derived from Palaeozoic sandstones in the northern upper Amazon Basin, Eur. J. Soil Sci., 55, 523–538, 2004.
Nascimento, N. R., Fritsch, E., Bueno, G. T., Bardy, M., Grimaldi, C., and Melfi, A.: Podzolization as a deferralitization process: dynamics and chemistry of ground and surface waters in an Acrisol – Podzol sequence of the upper Amazon Basin, Eur. J. Soil Sci., 59, 911–924, 2008.
Patel-Sorrentino, N., Lucas, Y., Eyrolles, F., and Melfi, A. J.: Fe, Al and Si species and organic matter leached off a ferrallitic and podzolic soil system from Central Amazonia, Geoderma, 137, 444–454, 2007.
RadamBrasil: Levantamento de Recursos Naturais, Ministério de Minas e Energia, Departa-

BGD
9, 2233–2276, 2012

mento Nacional de Produção Mineral, Rio de Janeiro, 1978.
Ravichandran, M., Aiken, G. R., Reddy, M. M., and Ryan, J. N.: Enhanced Dissolution of Cinnabar (Mercuric Sulfide) by Dissolved Organic Matter Isolated from the Florida Everglades, Environ. Sci. Technol., 32, 3305–3311, 1998.
Tardy, Y. and Nahon, D.: Geochemistry of laterites, stability of Al-goethite, Al-hematite, and Fe_3^+ kaolinites in bauxites and ferricretes: an approach to the mechanism of concretion formation, Am. J. Sci., 285, 865–903, 1985.
Tardy, Y., Roquin, C., Bustillo, V., Moreira, M., Martinelli, L. A., and Victoria, R.: Carbon and Water Cycles Amazon River Basin, Applied Biogeochemistry, Atlantica, Biarritz, 2009.
Veillon, L. and Soria-Solano, B.: Transition sol ferrallitique – podzol: cas d'une terrasse sédimentaire de l'Ucayali (Perou), Cah.ORSTOM, sér. Pédol., 24, 97–113, 1988.

BGD
9, 2233–2276, 2012

Table 1. Minerals identified in the soil material. Pits and horizon are located on Fig. 2.

Horizon	Depth (m)	Texture	Mineralogy				
			Quartz (%)	Kaolinite (%)	Gibbsite (%)	Muscovite (%)	Other minerals
Pit P1 – Podzol							
O and A1	0.0–0.8	Sand	88–95	2–12	ε-5	0-ε	A, R, Go, H
Es	0.8–1,9	Sand	100	ε	ε	0-ε	A, R, Go, H
Bh-Bhs	1.9–2.3	Sandy loam	90–94	6–10	ε	ε	A, R, Go, H
K1	2.3–4.0	Silty clay loam	ε-3	92–96	8–4	ε-1	A, M, Go, H
K2	4.0-10.0	Silty clay loam	ε-3	96–97	4–2	ε-1	A, M, Go, H
Pit P2 – Ferralsol							
A	0.0–0.3	Sandy clay loam	59–70	18–26	2–3	ε	A, V, Go
B1	0.3-1.3	Sandy clay loam/Clay loam	36–68	14–66	1–3	ε	A, V, R, Go
Ef	1.3–1.6	Silty clay loam	37	60	3	ε-1	Go
K1	1.6–3.0	Silty loam	6	94	ε	3–4	A, R,Go, H
K2	3.0–6.6	Silty loam	10	90	ε	2–6	A, R,Go, H
Pit P3 – Ferralsol							
A	0.0–0.1	Sandy clay loam	62	34	4	ε-1	A, R, Go
B2	0.1–1.0	Sandy clay	8–65	32–86	3–6	ε-1	A, R, Go
K3	1.0–1.3	Clay	10	86	4	1	A, Go, H
K1	1.3–4.0	Clay	2–9	86–92	5–8	1–2	A, R, Go, H
K4	4.0–5.6	Clay/Silty clay	2	96	2	2–13	A, R, Mc, Mg, Go, H
Pit P4 – Gleysol							
A	0.0–0.1	Sandy loam	59	24	1	3	A, R, Go, H
B3	0.1–1.4	Sandy loam	60–71	9–13	ε-1	3–7	A, R, Mc,Go, H
K4	1.4–2.7	Loam	42	15	ε	15	A, V, R, Mc, I, Go, H

A: anatase, M: muscovite, V: vermiculite, Mc: microcline, Mg: magnetite, I: illite, R: rutile, Go: goethite, H: hematite, ε: very small amounts.

BGD
9, 2233–2276, 2012

Table 2. Statistics of the composition of the groundwater for each sampling point.

	Si ($mg\,l^{-1}$)			Al^{3+} ($mg\,l^{-1}$)			Fe^{3+} ($mg\,l^{-1}$)			Fe^{2+} ($mg\,l^{-1}$)		
	av	max	min	av	max	min	av	max	min	av	max	min
Spring	0.05	0.07	0.02	0.02	0.05	< 0.01	0.01	0.05	0.00	< 0.05	0.10	< 0.05
CA2-20	0.05	0.10	0.02	0.03	0.14	< 0.01	0.03	0.07	0.00	0.06	0.13	< 0.05
CA1-150	0.27	0.48	0.19	0.18	0.24	0.14	0.04	0.15	0.00	0.10	0.38	< 0.05
P4-240	0.48	0.59	0.29	0.48	0.63	0.37	0.06	0.15	0.00	0.10	0.19	< 0.05
P4-510	0.13	0.20	0.10	0.37	0.41	0.33	0.02	0.03	0.00	0.07	0.20	< 0.05
PMVB-15	1.86	2.44	1.19	0.68	0.81	0.57	0.79	1.65	0.39	1.58	2.52	0.42
P13-160	0.46	0.57	0.31	0.20	0.27	0.17	0.04	0.08	0.02	0.21	0.63	< 0.05
P13-490	0.21	0.41	0.11	0.14	0.18	0.07	0.03	0.04	0.02	< 0.05	0.09	< 0.05
P12-160	0.30	0.40	0.21	0.06	0.09	0.04	0.01	0.04	0.00	0.05	0.15	< 0.05
P12-380	0.19	0.24	0.12	0.07	0.14	0.01	0.02	0.05	0.00	< 0.05	0.06	< 0.05
P6-400	0.49	0.71	0.25	0.03	0.07	< 0.01	0.07	0.46	0.01	< 0.05	0.07	< 0.05
P23-380	0.55	0.69	0.38	< 0.01	0.01	< 0.01	0.03	0.07	0.01	0.08	0.15	< 0.05
P24-80	0.29	0.56	0.15	0.63	0.76	0.50	0.06	0.11	0.01	0.15	0.48	< 0.05
P24-300	0.48	0.57	0.24	0.09	0.11	0.08	0.06	0.13	0.03	0.74	1.11	0.52

	pH			E_H (mV)			DOC ($mg\,l^{-1}$)		
	av	max	min	av	max	min	av	max	min
Spring	4.0	4.3	3.4	521	542	503	37	45	29
CA2-20	4.1	4.5	3.6	473	495	451	34	55	24
CA1-150	4.2	4.5	3.9	512	563	472	40	52	35
P4-240	4.1	4.4	3.5	501	567	410	15	19	12
P4-510	4.5	5.1	3.8	514	575	468	2	3	2
PMVB-15	4.6	5.1	4.0	372	415	325	32	38	27
P13-160	4.6	5.1	3.8	399	484	296	7	9	6
P13-490	4.6	5.1	3.9	499	543	444	4	7	2
P12-160	4.9	5.2	4.7	482	519	448	5	10	4
P12-380	4.9	5.2	4.6	494	532	467	4	6	2
P6-400	4.8	5.3	4.1	494	520	482	5	9	2
P23-380	4.9	5.4	4.3	460	478	437	3	5	2
P24-80	4.5	5.1	4.1	456	510	365	16	19	13
P24-300	5.0	5.5	4.4	172	191	147	5.4	9.7	3.5

BGD
9, 2233–2276, 2012

Table 3. Major ions charge, DOC and pH (average ± standard deviation).

Sampling point	Number of samples	Major ions charge						
		Na^{+} ($\mu eq\,l^{-1}$)	NH_4^{+} ($\mu eq\,l^{-1}$)	K^{+} ($\mu eq\,l^{-1}$)	Mg^{2+} ($\mu eq\,l^{-1}$)	Ca^{2+} ($\mu eq\,l^{-1}$)	Al^{*} ($\mu eq\,l^{-1}$)	Fe^{2+} ($\mu eq\,l^{-1}$)
Spring	4	24.7 ± 2.5	9.7 ± 4.5	8.9 ± 2.0	10.3 ± 3.0	103.0 ± 26.4	2.2 ± 2.6	1.0 ± 0.5
CA2-20	1	26.4	3.8	36.5	12.6	82.8	3.3	2.2
CA1-150	1	34.2	64.5	35.1	15.8	88.6	19.5	3.6
P4-240	4	30.2 ± 13.7	13.4 ± 19.1	19.7 ± 15.5	7.8 ± 2.7	46.4 ± 15.6	52.8 ± 4.5	3.6 ± 3.8
P4-510	4	14.8 ± 2.1	4.8 ± 6.1	5.0 ± 1.3	4.7 ± 1.4	34.7 ± 8.5	39.6 ± 3.4	2.2 ± 1.1
P13-490	4	27.6 ± 13.2	33.6 ± 28.2	8.7 ± 6.9	3.9 ± 1.4	53.2 ± 12.7	15.0 ± 5.5	1.4 ± 0.8
P6-400	4	36.9 ± 10.4	31.4 ± 19.4	43.2 ± 6.6	9.9 ± 1.4	73.9 ± 12.4	3.3 ± 2.3	1.4 ± 0.9
P24-300	4	18.1 ± 2.7	16.4 ± 10.0	30.4 ± 1.7	4.9 ± 0.5	61.6 ± 8.4	9.0 ± 5.2	26.4 ± 14.3
		Fe^{3*} ($\mu eq\,l^{-1}$)	Cl^{-} ($\mu eq\,l^{-1}$)	NO_2^{-} ($\mu eq\,l^{-1}$)	NO_3^{-} ($\mu eq\,l^{-1}$)	SO_4^{2-} ($\mu eq\,l^{-1}$)	pH**	DOC ($mg\,l^{-1}$)
Spring	4	0.6 ± 0.2	11.5 ± 4.1	0.0 ± 0.0	3.6 ± 6.2	11.1 ± 1.2	4.0 ± 0.08	37.4 ± 1.9
CA2-20	1	1.5	8.2	4.1	8.6	8.6	4.1	34.4
CA1-150	1	2.1	19.7	32.3	8.9	35.1	4.2	40.2
P4-240	4	3.9 ± 2.6	16.6 ± 9.9	0.0 ± 0.0	74.6 ± 10.8	24.2 ± 9.4	4.0 ± 0.09	15.2 ± 0.7
P4-510	4	1.2 ± 0.5	11.2 ± 2.8	2.0 ± 2.0	41.8 ± 7.2	17.4 ± 6.2	4.6 ± 0.08	2.3 ± 0.4
P13-490	4	1.5 ± 0.6	13.3 ± 9.7	0.0 ± 0.0	11.2 ± 5.1	22.8 ± 7.1	4.6 ± 0.13	4.0 ± 1.6
P6-400	4	3.9 ± 1.8	32.5 ± 18.1	3.9 ± 3.9	23.4 ± 10.4	34.7 ± 14.1	4.8 ± 0.07	4.9 ± 2.0
P24-300	4	3.3 ± 0.9	12.5 ± 1.1	0.0 ± 0.0	6.5 ± 4.6	15.0 ± 4.3	5.1 ± 0.17	5.4 ± 0.9

* Calculated for the sum of Al or Fe^{3} species, respectively.
** Values after correction, see text.

BGD
9, 2233–2276, 2012

Table 4. Result of modelling the microtitration curves by 4 discrete acidic site – pKa and site density L_T.

Spring				
pKa	3.5 ± 0.6	4.7 ± 0.4	6.9 ± 2.6	9.3 ± 1.5
L_T (meq gC^{-1})	17.2 ± 0.4	9.5 ± 0.4	8.1 ± 2.3	5.4 ± 5.6
CA1-150				
pKa	4.1 ± 0.3	5.2 ± 0.1	8.7 ± 0.1	10.6 ± 0.1
L_T (meq gC^{-1})	10.9 ± 0.3	7.1 ± 0.5	2.6 ± 0.3	6.6 ± 3.5

BGD
9, 2233–2276, 2012

Table 5. Calculated charge due to DOM and acid site density for various pKa.

Sampling point	Number of samples	Sum of charges of major ions $\sum_i Z_i$ (μeq l^{-1})	pH	DOC (μeq l^{-1})	Charge due to DOM Z_{DOM} (meq gC^{-1})	Acid-site density $L_T$meq gC^{-1} pKa			
						3.0	3.5	4.0	4.5
Spring	4	134 ± 28	4.0 ± 0.08	37.4 ± 2.9	−6.3 ± 1.8	7 ± 2	8 ± 3	13 ± 5	26 ± 11
CA2-20	1	142	4.1	34.4	−6.5	7	8	12	23
CA1-150	1	184	4.2	40.2	−6.2	7	7	10	19
P4-240	4	59 ± 36	4.0 ± 0.09	15.2 ± 0.7	−11 ± 4	12 ± 4	14 ± 6	22 ± 10	46 ± 22
P4-510	4	33 ± 3	4.6 ± 0.08	2.3 ± 0.4	−31 ± 4	31 ± 4	33 ± 5	38 ± 7	55 ± 12
P13-490	4	98 ± 39	4.6 ± 0.13	4.0 ± 0.7	−37 ± 13	38 ± 14	40 ± 15	47 ± 18	67 ± 29
P6-400	4	109 ± 29	4.8 ± 0.07	4.9 ± 2.0	−32 ± 8	33 ± 8	34 ± 9	37 ± 10	48 ± 15
P24-300	4	135 ± 27	5.1 ± 0.17	5.4 ± 0.9	−32 ± 5	32 ± 5	33 ± 5	34 ± 6	40 ± 8

BGD
9, 2233–2276, 2012

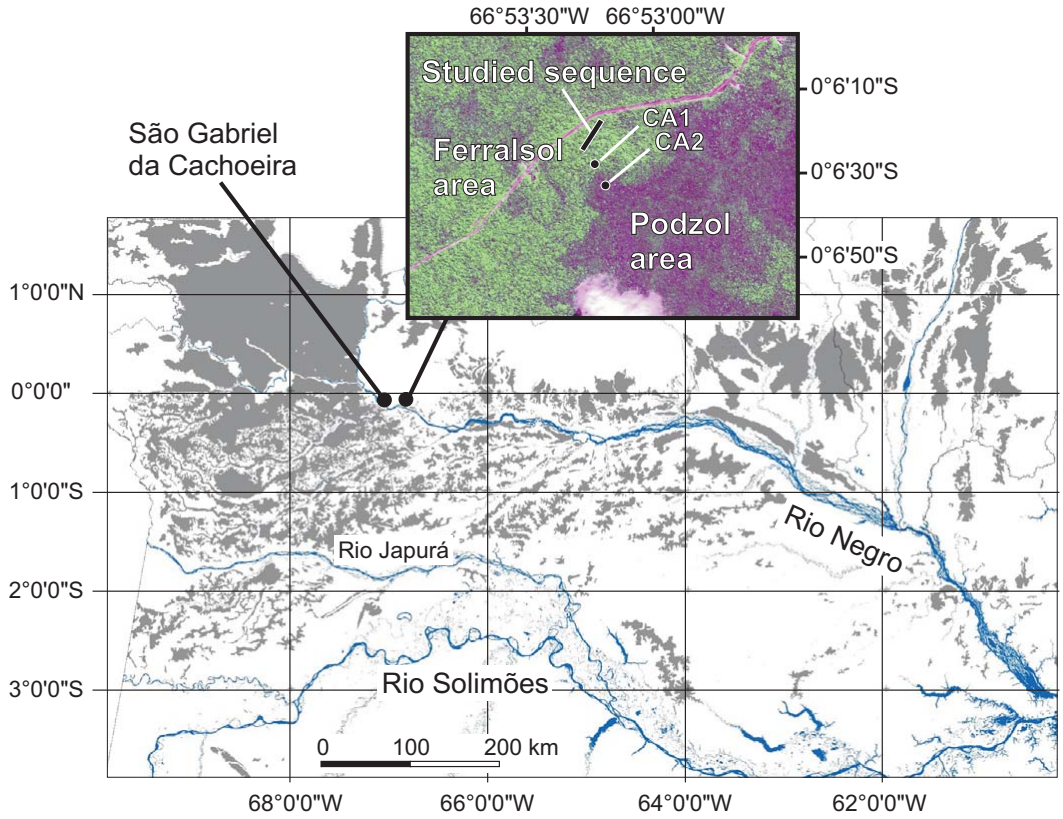

Fig. 1. Situation of the studied sequence and extension of highly podzolic areas (in grey) in the Rio Negro basin. Compilation of highly podzolic areas was realized from digitalized soil maps of Amazonia (IBGE, 2009). The detailed view of the studied area is issued from IKONOS imagery, the darker forested area corresponds to closed, low forest over hydromorphic podzols. CA1 and CA2 are sampling points outside the sequence.

BGD
9, 2233–2276, 2012

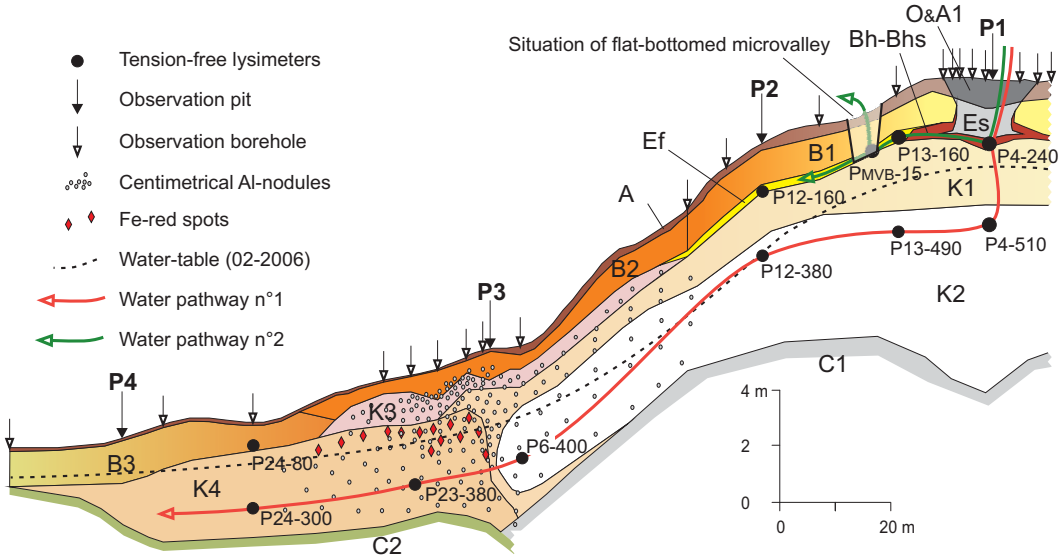

Fig. 2. View of the soil system along the catena. Capital letters of horizon names refer to the FAO terminology. O: organic, peat-like horizon; A1: organic-rich, dark brown horizon; A: horizons brown-coloured by organic matter; Es: podzolic eluviated horizons; B1: oxic B horizons varying from sandy upslope to sandy-clayey downslope; B2: oxic sandy-clay B horizons; B3: pseudogley B horizons; K: kaolin horizons; Bh-Bhs: horizons with organic matter and Al-Fe accumulation; Ef: non podzolic leached horizon; C1 and C2: saprolitic horizons. P1 to P4: situation of mineralogical data given in Table 1.

BGD
9, 2233–2276, 2012

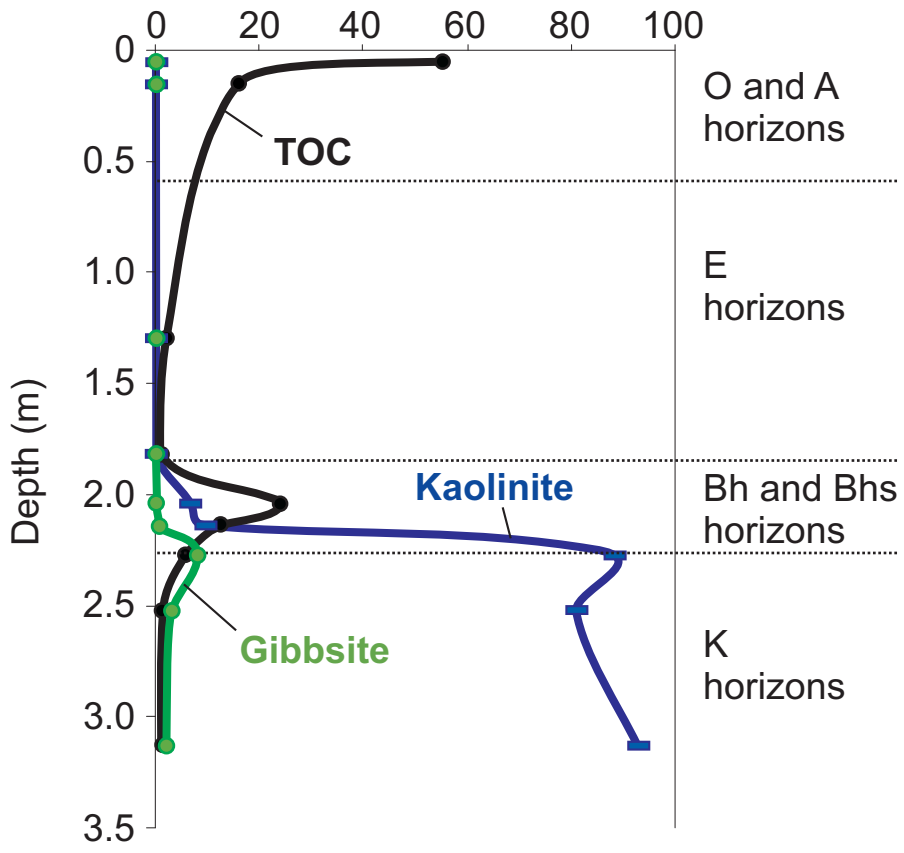

Fig. 3. Kaolinite, gibbsite and total organic carbon (TOC) in the podzol from the upper part of the catena. Horizontal axis is in % for kaolinite and gibbsite and in ‰ for TOC.

BGD
9, 2233–2276, 2012

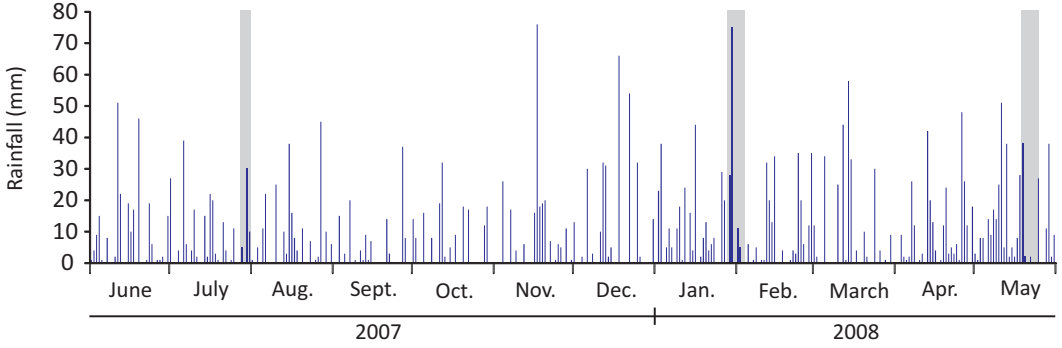

Fig. 4. Daily rainfall in the area. Grey vertical bars indicate the sampling periods.

BGD
9, 2233–2276, 2012

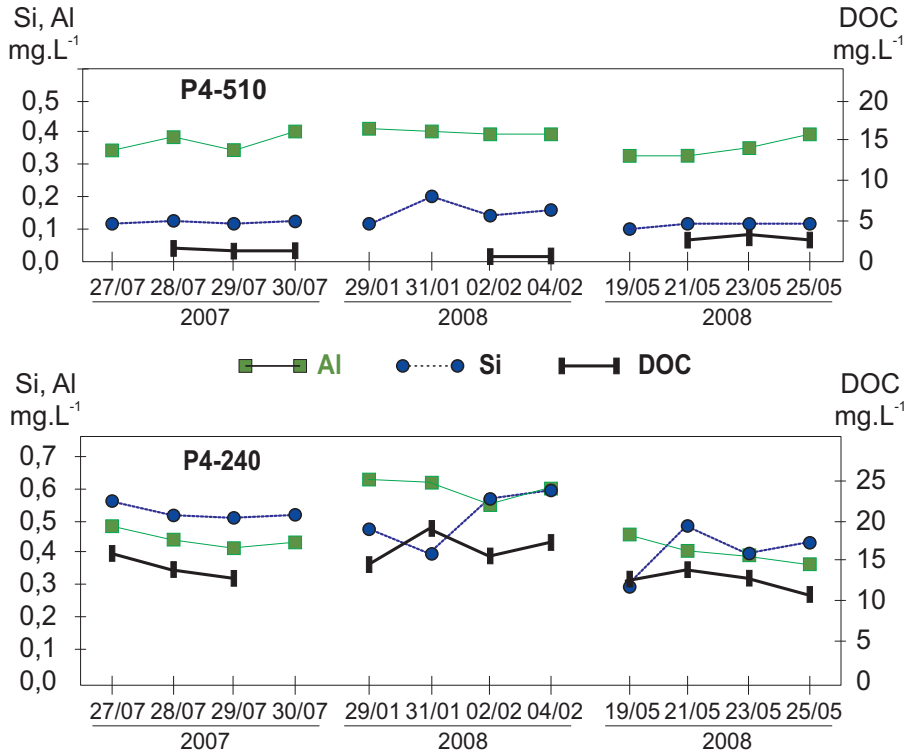

Fig. 5. H_4SiO_4, Al^{3+}, and DOC concentrations of filtered waters sampled at points P4-510 and P4-240.

BGD
9, 2233–2276, 2012

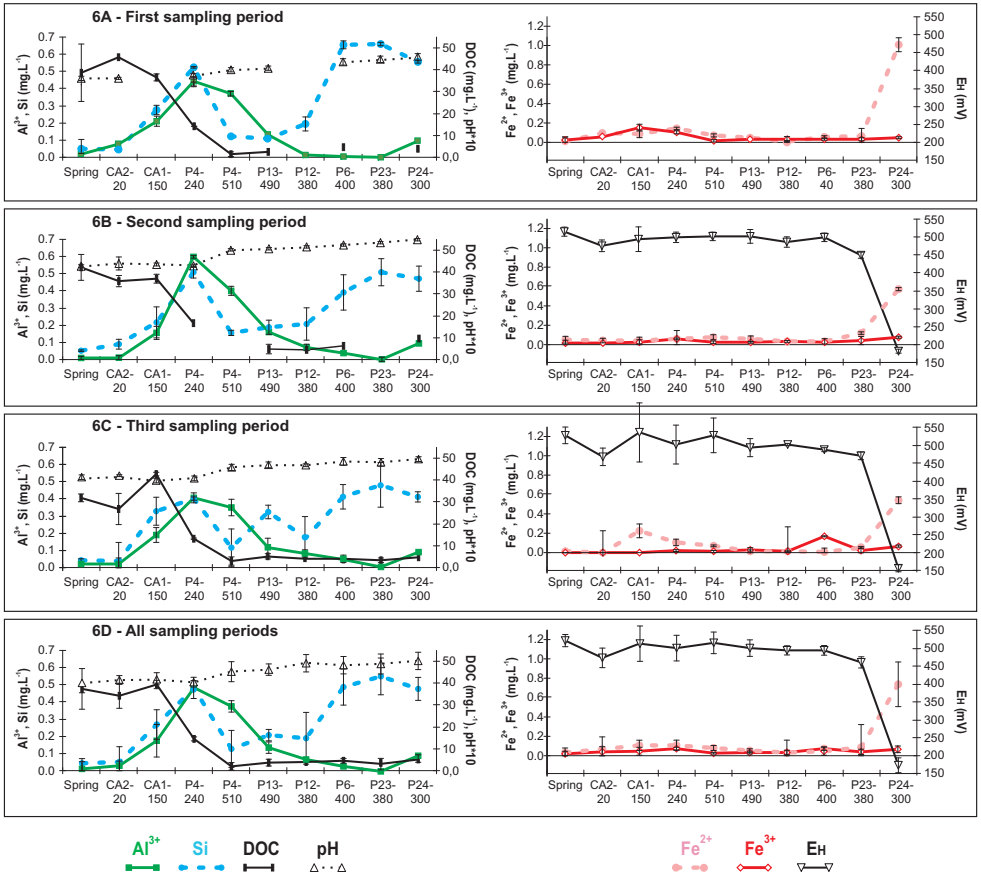

Fig. 6. Average composition of the sampled waters along the pathway no. 1 for each sampling period **(A–C)** and overall average **(D)**. Vertical bars give the calculated standard deviation for each set of data.

BGD
9, 2233–2276, 2012

Biogeochemistry of an amazonian podzol-ferralsol soil system

Y. Lucas et al.

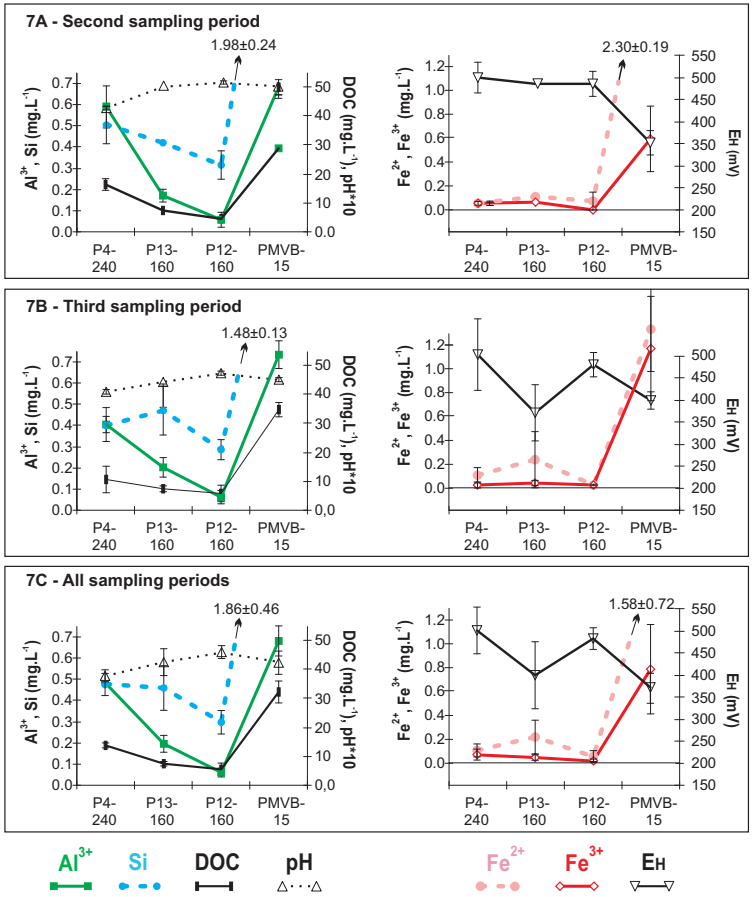

Fig. 7. Average composition of the sampled waters along the pathway no. 2 for the second and the third sampling periods **(A)** and **(B)** and overall average **(C)**. Vertical bars give the calculated standard deviation for each set of data.

BGD
9, 2233–2276, 2012

Biogeochemistry of an amazonian podzol-ferralsol soil system

Y. Lucas et al.

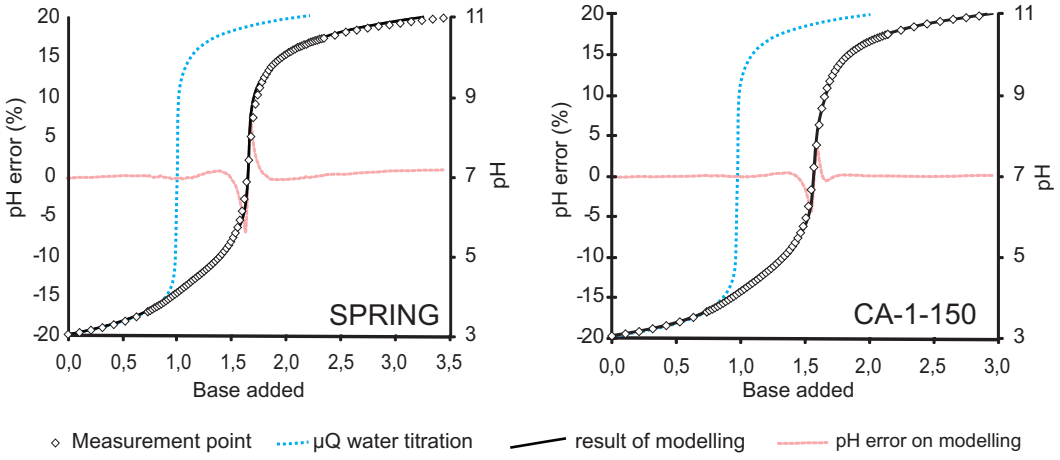

Fig. 8. Microtitration curves of DOM-rich grounwaters and result of modelling with the PROCESE software.

BGD
9, 2233–2276, 2012

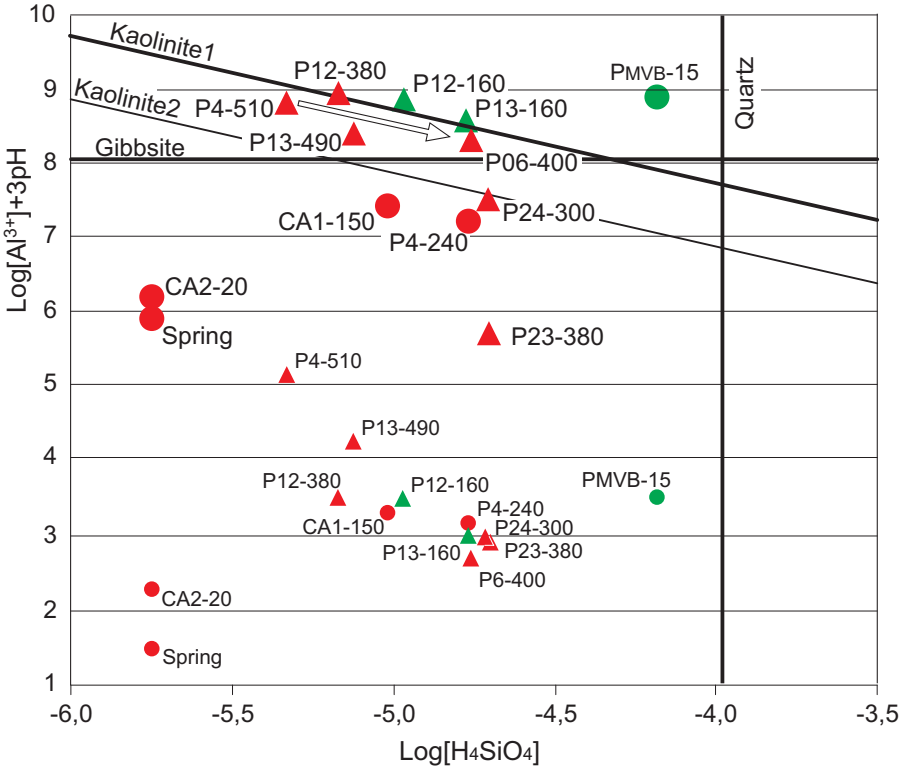

Fig. 9. Position of the groundwaters in the Si-Al system calculated from the average compositions. Larger and smaller symbols give groundwaters without, or with considering complexation by DOM, respectively. Red and green symbols indicate groundwaters following pathway no. 1 and no. 2, respectively, triangular symbols indicate groundwaters supposed to be controlled by kaolinite dissolution/precipitation and circles indicate groundwaters with high DOC.

BGD
9, 2233–2276, 2012

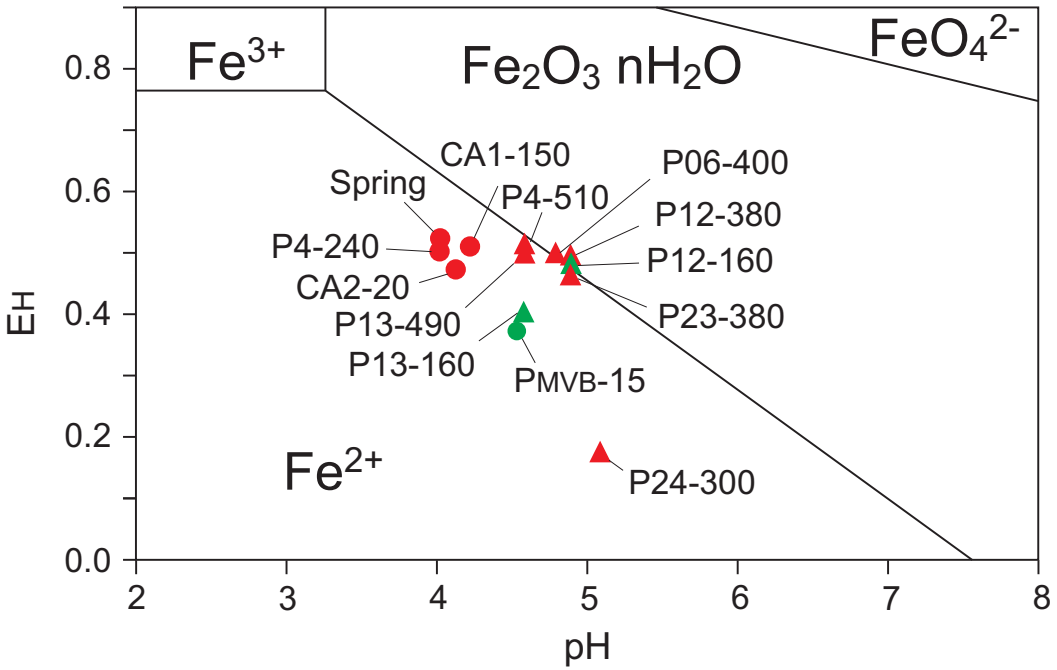

Fig. 10. Position of the groundwaters in the iron Pourbaix diagram drawn for low Fe-concentrated waters ($<10^{6}$ M). Symbols are the same that in Fig. 9.

BGD
9, 2233–2276, 2012